Journal of Organometallic Chemistry, 449 (1993) 147–157

JOM 23370

Synthesis and characterization of sterically encumbered Li, Na, and K aryl tellurolates, and some Pt(II), Ir(I), and Cd(II) derivatives

Philip J. Bonasia and John Arnold

Department of Chemistry, University of California, Berkeley, CA 94720 (USA)

(Received August 3, 1992)

Abstract

The synthesis, isolation, and characterization of several alkali metal aryl tellurolates of general formula (2,4,6-$R_3C_6H_2$)TeM(sol)$_n$ (R = Me, ^{i}Pr, ^{t}Bu; M = Li, Na, K; sol = THF, n = 1.33, 1.5, 2.5, 3; sol = DME, n = 1; sol = TMEDA, n = 1; sol = 18-crown-6, n = 1) is reported. Reduction of (2,4,6-$Me_3C_6H_2)_2Te_2$ and (2,4,6-$^iPr_3C_6H_2)_2Te_2$ with 2 equiv of $LiEt_3BH$ in THF affords the corresponding lithium tellurolates **1** and **2**. Direct Te insertion into the C–Li bond of (2,4,6-$^tBu_3C_6H_2$)Li(THF)$_3$ in THF produces **3**, while a similar reaction of Te metal with (o-$C_6H_4CH_2NMe_2$)Li affords the chelating tellurolate, **4**. The action of Na/Hg amalgam on THF solutions of (2,4,6-$Me_3C_6H_2)_2Te_2$ or (2,4,6-$^iPr_3C_6H_2)_2Te_2$ followed by work-up with TMEDA or DME leads to the sodium tellurolates **5** and **6** respectively. Treatment of THF solutions of (2,4,6-$^iPr_3C_6H_2)_2Te_2$ with 2 equiv. of K^sBu_3BH gives the polymeric tellurolate, (2,4,6-$^iPr_3C_6H_2)_2$TeK(THF)$_{1.33}$, (**7**). The infinite ladder-like structure is broken by reaction with 18-crown-6, which affords the monomeric derivative, **8**. Reaction of **2** or **3** with THF suspensions of *cis*-$(PPh_3)_2PtCl_2$ produces the air-stable *cis*-platinum tellurolates, **9** and **10**, respectively. Reaction of **3** with *trans*-$(PPh_3)_2$Ir(CO)Cl, leads to the isolation of **11**, a rare example of a Vaska's type complex with a *cis*-geometry, and only the second such structurally characterized derivative. Reaction of **4** with 1/2 equiv. of $CdBr_2$ produces **12**, Cd[Te(o-$C_6H_4CH_2NMe_2$)]$_2$. Compounds **3**, **4**, **7**, **10**, and **11** have been characterized by single crystal X-ray diffraction.

1. Introduction

Recent interest in the chemistry of tellurolate derivatives [1–10] has, for the most part, been directed toward synthesis of semiconductor materials incorporating tellurium [11–20]. Steigerwald has prepared complexes such as $M(ER)_2$ (M = Zn, Cd, Hg; E = S, Se, Te; R = n-butyl, phenyl, 4-methylphenyl), which decompose thermally according to eqn. (1) [11–14]:

$$M(ER)_2 \longrightarrow ME + ER_2 \qquad (1)$$

By varying pyrolysis conditions, bulk and nanocluster II–VI compounds were obtained. Bochmann has shown that *in situ* preparation of aryl tellurols followed by low temperature manipulation and reaction with Group 12 amides affords the aryl tellurolates of cadmium and mercury [16,21]. In the case of [Cd(2,4,6-$Me_3C_6H_2$-Te)$_2]_\infty$, polycrystalline CdTe was produced by thermal decomposition in refluxing mesitylene [21]. In similar preparations, samples of the II–VI semiconductors ZnSe, CdS, CdSe, and HgS, have been isolated [16,17,22]. Bianconi has extended this approach to lanthanide(II) complexes and has shown that these species also decompose according to eqn. (1) [19].

The vast majority of alkali metal aryl tellurolates that have been prepared used as tellurolating synthons *in situ* [23]. Nevertheless, Klar has prepared and isolated base free NaTePh and KTePh, [24] while Du Mont had previously isolated the THF-coordinated lithium supermesityl (supermesityl = 2,4,6-$^tBu_3C_6H_2$) tellurolate that we also report here [2]. Base free KTe(2,4,6-$Me_3C_6H_2$), has also been prepared [19].

Recently we reported several examples of stable, easily isolable, sodium and potassium salts of sterically hindered aryl tellurolates [6]. Here we present a full account of this work and we show how these compounds may be used in salt-elimination reactions to produce several platinum tellurolates, a rare example of a *cis*-Vaska's type compound, and a cadmium complex incorporating a novel chelating tellurolate ligand.

Correspondence to: Dr. J. Arnold.

0022-328X/93/$6.00

2. Results and discussion

2.1. Isolation and characterization of tellurolate anions

Insertion of tellurium into reactive alkali metal–carbon bonds is a well-established synthetic route for the *in situ* preparation of alkyl and aryl tellurolate anions [23]; however, in most instances these reactions are complex and the resulting solutions contain a mixture of products that are difficult to purify. We [6] and others [25,26] have shown that, in some cases, pure products are best obtained in two further steps, whereby the reaction mixture is oxidized to the ditelluride (which is air-stable and readily purified), followed by a clean reduction step. For example, reduction of $(2,4,6\text{-}Me_3C_6H_2)_2Te_2$, $(2,4,6\text{-}^iPr_3C_6H_2)_2Te_2$, or $(2,4,6\text{-}^tBu_3C_6H_2)_2Te_2$, with 2 equiv. of $LiEt_3BH$ in THF leads to the corresponding lithium tellurolates $(2,4,6\text{-}Me_3C_6H_2)TeLi(THF)_{1.5}$ (**1**), $(2,4,6\text{-}^iPr_3C_6H_2)TeLi(THF)_{2.5}$ (**2**), and $(2,4,6\text{-}^tBu_3C_6H_2)TeLi(THF)_3$ (**3**). In **1** and **2**, THF is labile, and vacuum dried samples show 1.5 and 2.5 THF/Li respectively, on ^1H NMR spectroscopic investigation. The bulky supermesityl tellurolate, **3**, was first isolated by Du Mont and, until only a few years ago, it remained the literature's only example of an isolable lithium tellurolate [2]. The molecular structure of **3** is shown as an ORTEP view in Fig. 1; pertinent bond distances and angles are given in Table 1. Overall, the structure is reminiscent of those previously described for $(2,4,6\text{-}Me_3C_6H_2)TeNa(TMEDA)_2$ (**5**) and $(2,4,6\text{-}^iPr_3C_6H_2)TeK(18\text{-crown-}6)$ (**8**) [6]. In **3** the *ipso*-carbon–Te–M angle is 99.1(2)° compared to corresponding angles in **5** and **8** of 102.26(5)° and 77.68(7)°, respectively. The aryl ligand in **3** is quite planar with C1–C6 deviating by ±0.05 Å. The Te atom is 0.56 Å out of this plane, displaced in the direction of the Li atom. This displacement may be caused by intramolecular interaction between the Te atom and the t-butyl groups, which shows six contacts (C7, C8, C9, C15, C16 and C18) in the range of 3.55 Å, or it may be due to the overall packing effects. This latter effect seems more probable, as inspection of the same six long range contacts in the structures of *cis*-$(PPh_3)_2Pt[Te(2,4,6\text{-}^tBu_3C_6H_2)]Cl$ (**10**) and *cis*-$(PPh_3)_2Ir[Te(2,4,6\text{-}^tBu_3C_6H_2)](CO)$ (**11**) discussed below, shows that as the Te-to-t-butyl group contacts become longer, the Te deviation out of plane becomes larger. This trend is the opposite of what would be expected if these "repulsive" contacts *alone* were pushing the Te atom out of the aryl plane. The quaternary carbons in the *ortho* t-butyl groups, C7 and C15, are displaced out of the aryl ring plane away from the Te atom by 0.16 and 0.17 Å respectively. The quaternary carbon in the *para* t-butyl group (C11), is displaced 0.05 Å out of the aryl plane toward the Te atom.

The oxidation/reduction route, though tedious, appears to be the best method for preparation of the tellurolate anions. Nonetheless, in two cases, direct insertion of Te metal into the C–Li bond of $(2,4,6\text{-}^tBu_3C_6H_2)Li(THF)_3$ and $(o\text{-}C_6H_4CH_2NMe_2)Li(THF)_3$ in THF affords the tellurolate anions, **3** and (*o*-

TABLE 1. Selected bond distances (Å) and angles (deg) for **3**

Te–C1	2.184(4)	Te–Li	2.82(1)
C1–C2	1.441(6)	C1–C6	1.420(6)
C2–C3	1.404(6)	C3–C4	1.370(7)
C4–C5	1.374(6)	C5–C6	1.388(6)
Li–O1	1.93(1)	Li–O2	1.95(1)
Li–O3	1.97(1)		
C1–Te–Li	99.1(2)	Te–C1–C2	119.9(3)
Te–C1–C6	121.1(3)	C2–C1–C6	118.4(4)
C1–C2–C3	118.0(4)	C1–C2–C7	125.7(4)
C3–C2–C7	116.3(5)	C2–C3–C4	123.4(5)
Te–Li–O1	114.8(4)	Te–Li–O2	108.8(5)
Te–Li–O3	115.2(4)		

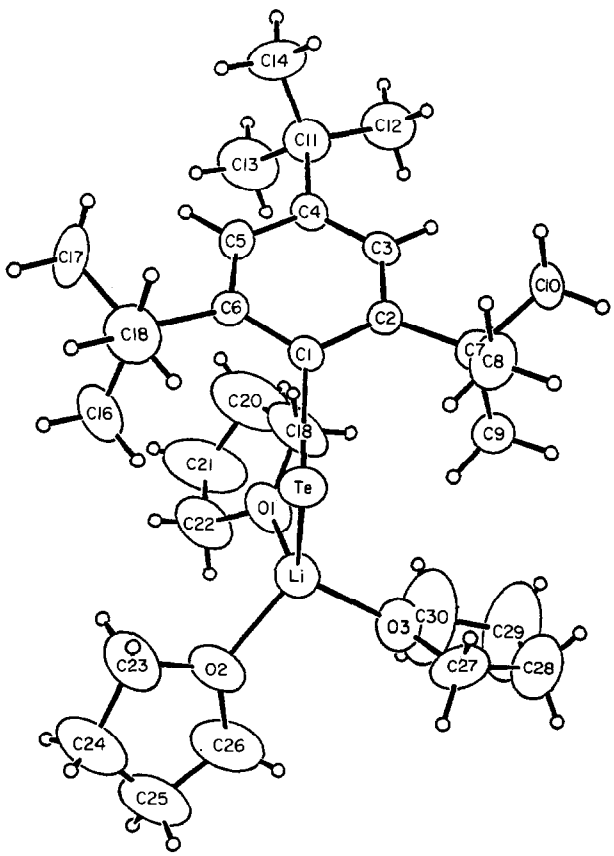

Fig. 1. ORTEP view of the molecular structure of $(2,4,6\text{-}^tBu_3C_6H_2)TeLi(THF)_3$ (**3**). Thermal ellipsoids are scaled to represent the 50% probability surface. Hydrogen atoms are given as arbitrary small spheres for clarity.

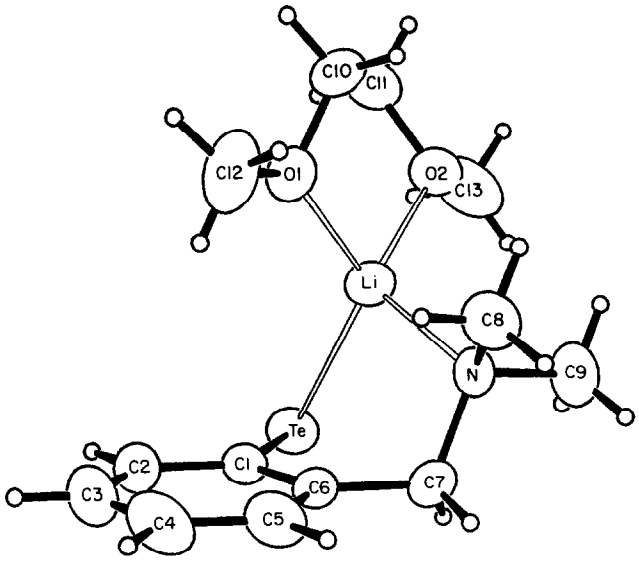

Fig. 2. ORTEP view of the molecular structure of $(o\text{-}C_6H_4CH_2NMe_2)$-TeLi(DME) (**4**). Thermal ellipsoids are scaled to represent the 50% probability surface. Hydrogen atoms are given as arbitrary small spheres for clarity.

$C_6H_4CH_2NMe_2)$TeLi(DME) (**4**), respectively, in reasonable yields following a brief work-up.

The aminotolyl tellurolate, **4**, is, we believe, the first example of a tellurolate ligand that is intramolecularly coordinated via a heteroatom donor. We note, however, that a wide variety of chelating telluroethers have been known for many years [27–30]. An ORTEP view of **4** is shown in Fig. 2, with selected bond distances and angles given in Table 2. The C–Te–Li angle, 70.6(1)°, is remarkably acute, and again seems to demonstrate that the R–Te$^-$ moiety has little directional character. The Li atom is tetrahedrally coordinated by the two DME oxygens, the aryl-amine nitrogen, and the Te atom. Compared to the relatively long Te–Li distance of 2.82(1) Å observed in **3**, the Te–Li distance of 2.717(4) Å is closer to that predicted by covalent radii [31]. The Te–C distance, 2.142(2) Å, is normal. The six carbons in the phenyl ring are co-planar, deviating by

TABLE 2. Selected bond distances (Å) and angles (deg) for **4**

Li–Te	2.717(4)	Li–O1	1.953(4)
Li–O2	1.943(4)	Li–N	2.040(5)
Te–C1	2.142(2)	C1–C2	1.390(4)
C1–C6	1.409(3)	C2–C3	1.375(4)
C3–C4	1.371(4)	C4–C5	1.385(4)
C5–C6	1.392(4)	C6–C7	1.502(3)
Te–Li–O1	125.8(2)	Te–Li–O2	118.2(2)
Te–Li–N	99.6(2)	O1–Li–O2	85.6(2)
O1–Li–N	116.6(2)	O2–Li–N	111.6(2)
Li–Te–C1	70.6(1)		

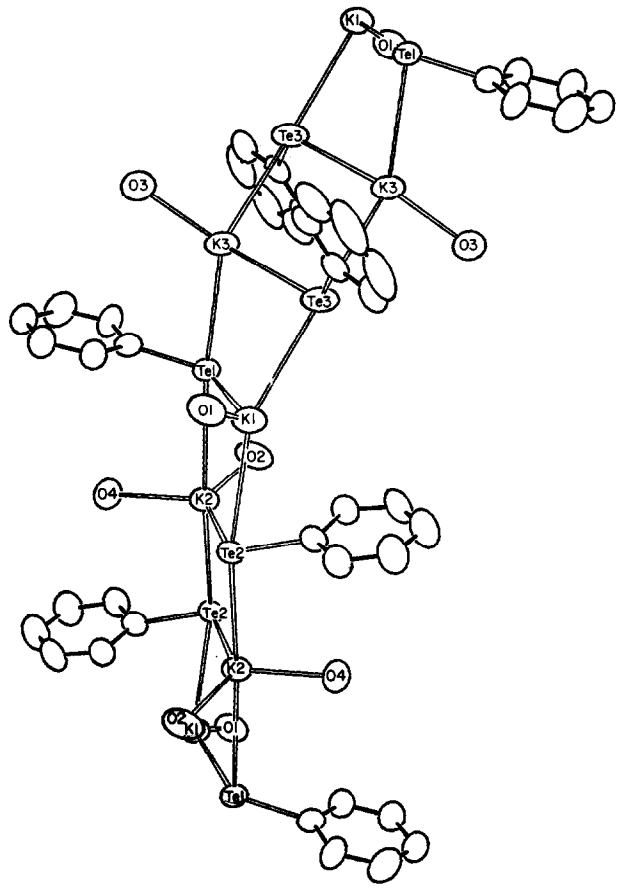

Fig. 3. ORTEP view of the molecular structure of (2,4,6-$^i Pr_3C_6H_2$)TeK(THF)$_{1.33}$ (**7**). Thermal ellipsoids are scaled to represent the 50% probability surface. THF carbon atoms and the aryl ligand isopropyl groups are omitted for clarity.

±0.01 Å. From this plane, the Te atom is displaced 0.10 Å *away* from the Li atom. There are no apparent close contacts between the molecules.

Treatment of $(2,4,6\text{-}Me_3C_6H_2)_2Te_2$ with Na/Hg amalgam, followed by reaction with TMEDA affords **5**, while similar reactions with $(2,4,6\text{-}^iPr_3C_6H_2)_2Te_2$ lead to isolation of (2,4,6-$^i Pr_3C_6H_2$)TeNa(DME) (**6**). The X-ray crystal structure of **5** was described earlier [6].

The unusual potassium salt (2,4,6-$^i Pr_3C_6H_2$)-TeK(THF)$_{1.33}$ (**7**) results from the action of 2 equiv. of K^{s}Bu$_3$BH on $(2,4,6\text{-}^iPr_3C_6H_2)_2Te_2$ in THF. The molecular structure of **7** is shown as an ORTEP view in Fig. 3, with pertinent bond lengths and angles given in Table 3. The K and Te atoms form a series of infinite "ladders" of nearly square planes of alternating Te and K atoms. The compound crystallizes in space group $P\bar{1}$, and the inversion center is clearly seen in the centers of both $(Te2)_2(K2)_2$ and $(Te3)_2(K3)_2$ cores. Each Te atom is coordinated by its *ipso* aryl carbon and three K atoms in a near trigonal bipyramidal (tbp) geometry; a lone pair of electrons presumably occupies the third equatorial site. The tbp geometry, however, is

TABLE 3. Selected bond distances (Å) and angles (deg) for 7

K1–Te1	3.570(2)	K2–Te1	3.562(2)
K3–Te1	3.393(2)	K1–Te2	3.419(2)
K2–Te2	3.683(2)	K2–Te2	3.548(2)
K1–Te3	3.446(2)	K3–Te3	3.476(2)
K3–Te3	3.446(2)	Te1–C1	2.15(1)
Te2–C16	2.162(7)	Te3–C31	2.15(1)
K1–O1	2.661(5)	K2–O2	2.810(9)
K2–O4	2.633(5)	K3–O3	2.633(6)
K1–Te1–K2	86.54(4)	K1–Te1–K3	91.39(4)
K2–Te1–K3	174.35(5)	K1–Te1–C1	113.9(3)
K2–Te1–C1	105.4(2)	K3–Te1–C1	80.2(2)
Te1–K1–Te2	92.12(4)	Te1–K1–Te3	79.14(3)
Te1–K1–O3	130.8(1)	Te2–K1–Te3	152.13(6)
Te2–K1–O1	105.4(1)	Te3–K1–O1	98.8(1)

not very regular with the primary deviations being the axial K–Te–K angle (from 161.84(7)° to 174.35(5)°), the angles from the axial K to the equatorial C (from 70.1(2)° to 107.8(2)°), and the K–Te distances, which vary from 3.41 to 3.68 Å. These distances show no pattern with respect to coordination environment, implying that the K–Te bond is largely ionic in character and that the coordination distances are controlled by inter-ligand contacts. There are, however, no particularly short inter-molecular contacts observed, and it seems that the overall packing determines the structure. The Te–C bonds are all very similar (2.15 to 2.16 Å). The coordination geometries of the K atoms are not regular. Each is coordinated by three Te atoms and either one or two THF oxygen atoms, perhaps suggesting that compared to similar Li and Na tellurolates, the larger and softer K prefers donation from the softer Te atoms on adjacent molecules rather than the harder O atoms in THF. As with the Te atoms, the geometry about each K atom may be described as trigonal bipyramidal; the geometry around K2 most closely approximates that of tbp geometry, while those about K1 and K3 are severely distorted. In the monomeric potassium tellurolate **8** we described previously [6], each potassium atom clearly achieves its common coordination number of eight; the potassium is bound by six oxygens from the crown ether, and by Te. The eighth coordination site is filled by a compressed aryl ring on a second tellurolate molecule below the crown ether plane. In **7** the vacant coordination sites on potassium are taken up at long distances by the steric crowding of aryl isopropyl groups and THF methylene groups. We also note that the second THF molecule bound to K2 is disordered, as is the *beta* carbon on the *para* isopropyl group of Te3. These disorders were appropriately modeled and presented no further difficulties.

2.2. Metal complexes with bulky tellurolate ligands

Reaction of **2** or **3** with *cis*-$(PPh_3)_2PtCl_2$ in THF affords good yields of *cis*-$(PPh_3)_2Pt[Te(2,4,6\text{-}^iPr_3C_6H_2)]Cl$ (**9**) as a pink-red powder, and **10** as purple-red, air-stable crystals respectively. Solutions of **9** and **10** are sensitive to normal room lighting or sunlight, becoming pale brown over several hours. The nature of this photodecomposition is unclear, but we note that free triphenylphosphine and ditelluride are the major decomposition products.

$^{31}P\{^1H\}$ NMR measurements of **9** and **10** are nearly identical and reveal the *cis* nature of these two platinum derivatives. The spectra show an AB pattern ($\delta \approx 17$ ppm; $J(PP) \approx 17$–18 Hz) with each major resonance being flanked by ^{195}Pt satellites (^{195}Pt; $I = 1/2$, 33.8%). Two distinct $^1J(P\text{–}Pt)$ values are observed for each compound (**9**, $^1J(P\text{–}Pt) = 2507$, 3876 Hz; **10**, $^1J(P\text{–}Pt) = 2478$, 3934 Hz). On the basis of $^1J(P\text{–}Pt)$ observed for *cis*-$(PPh_3)_2PtCl_2$ (3670 Hz), we assign the larger coupling constants in **9** and **10** to the phosphorus *trans* to the Pt–Cl bond [32]; the smaller coupling is then assigned to the Pt–P bond *trans* to the tellurolate ligand. Assuming the magnitude of this coupling scales inversely with the 6s character in the Pt–X bond *trans* to phosphorus [33], we conclude that the tellurolate ligand has a higher *trans*-influence than the chloride. Single crystal X-ray diffraction data further substantiate the greater *trans*-influence of the tellurolate ligand.

Figure 4 shows an ORTEP view of **10**, with selected bond distances and angles given in Table 4. The structure consists of molecules of the compound packed in the unit cell with molecules of toluene occupying holes in the packing. The closest approach between molecules (< 3.5 Å) is between phenyl groups of the triphenylphosphine moieties and are of the π-stacking type.

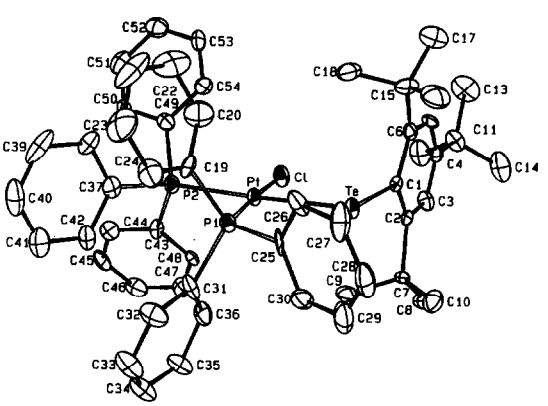

Fig. 4. ORTEP view of the molecular structure of *cis*-$(PPh_3)_2Pt[Te(2,4,6\text{-}^tBu_3C_6H_2)]Cl$ (**10**). Thermal ellipsoids are scaled to represent the 50% probability surface.

TABLE 4. Selected bond distances (Å) and angles (deg) for **10**

Pt–Te	2.614(1)	Pt–Cl	2.353(3)
Pt–P1	2.237(3)	Pt–P2	2.332(3)
Te–C1	2.17(1)	C1–C2	1.39(2)
C1–C6	1.45(2)	C2–C3	1.40(2)
C2–C7	1.61(2)	C3–C4	1.37(2)
C4–C5	1.36(2)	C4–C11	1.56(2)
C5–C6	1.38(2)	C6–C15	1.52(2)
Te–Pt–Cl	91.96(8)	Te–Pt–P1	86.00(9)
Te–Pt–P2	177.85(9)	Cl–Pt–P1	176.9(1)
Cl–Pt–P2	86.7(1)	P1–Pt–P2	95.4(1)
Pt–Te–C1	105.5(3)		

There are apparently no close interactions involving the atoms of the Te-aryl ligand. The Pt(II) center is square planar; the least squares plane deviates by only ±0.04 Å from planarity. There is an obvious *trans* influence in that the Pt–P distances are different by 0.10 Å (Pt–P1 2.237(3) Å, Pt–P2 2.332(3) Å); these data confirm the $^{31}P\{^1H\}$ NMR measurements discussed above. Comparing the distances to the isoelectronic structure of **11** discussed below, however, we find that the longer M–P distance is *trans* to the Tc in the Pt structure and *cis* to the Te in the Ir structure. The longer M–P distance is essentially the same in both structures, as is the M–Te distance. The Pt–Cl distance of 2.353(3) Å is rather short compared to a number of other *trans*-platinum compounds, $(PPh_3)_2$-PtLCl, where L is methyl [34], allyl [35], or phenyl [36], but this is expected as alkyl and phenyl ligands are among the strongest *trans* influence ligands. In *cis*-$(PPh_3)_2Pt(CF_2COCF_2Cl)Cl$, the Pt–Cl bond distance is 2.349 Å [37]. In the Te–aryl ligand, C1 is 0.20 Å out of the Pt plane, and the plane of the aryl ligand is perpendicular to the Pt plane. The aryl ligand is quite planar, with deviations of the six central carbons of only ±0.03 Å. The Te is displaced 0.28 Å from this aryl plane, in the direction of the Pt atom; the quaternary carbons of the butyl groups are displaced by 0.22, 0.07, and 0.11 Å for C7, C11, and C15 respectively. The *ortho* carbons, C2 and C6 are displaced away from the Te by 0.03, and 0.01 Å respectively, while the *para* carbon, C4, is displaced towards the Te atom by 0.02 Å. This is the same pattern of deviations from planarity observed in the structures of **11** and **3**. It is interesting that the deviations in the three cases are grossly different, with the tellurolate ligand in **10** being closest to planar in all respects and that in **11** being the furthest from planarity. In all three cases the Te–C1 bond length appears to be unchanged at 2.17 to 2.18 Å. It would appear that the aryl carbons of this system are very flexible. A number of other platinum aryltellurolates and selenolates have been prepared [38,39], and two have been structurally characterized. In $Pt(Te_2C_6H_4)(PPh_3)_2$ [40], the Pt–Te bond lengths are 2.586 and 2.592 Å, and the bridging tellurolate ligand in $Pt_2Cl_2(\mu\text{-}Cl)(\mu\text{-}TePh)(PBu_3)_2$ [41], shows Pt–Te distances of 2.531 and 2.532 Å. The longer Pt–Te bond length in **10** (2.614(1) Å) may simply reflect increased intraligand repulsions resulting from the presence of bulky *ortho*-t-butyl groups on the phenyl moiety. In the telluroether derivative, $[Pt\{PhTe(o\text{-}PPh_2C_6H_4)\}_2][Pt(SCN)_4] \cdot 2DMF$, the Pt–Te distance is 2.575 Å [27], and in the telluride, $(PPh_3)_2Pt(\mu\text{-}Te)_2Pt(PPh_3)_2$, the Pt–Te bond lengths are 2.612 and 2.628 Å [42].

Reaction of 1 equiv of **3** with Vaska's compound in ether leads to the formation of **11** as red needles in good yield. This compound represents one of only a handful of Vaska's derivatives with *cis*-geometries. Dahlenburg has prepared the only other examples of *cis*-$(PPh_3)_2Ir(L)(CO)$, where L is 2,4,6-$Me_3C_6H_2$ [43], 2,6-$Me_2C_6H_3$ [44], 2,6-$Et_2C_6H_3$ [45], 2-Et-6-MeC_6H_3 [45], Me_3SiCH_2 [46], or Me_3CCH_3 [46]. With the exception of the mesityl derivative, *cis–trans* isomerism occurs in each of these compounds as shown by ^1H and ^{31}P NMR spectroscopy. In addition, both *cis* and *trans*-$(PPh_3)_2Ir(2,4,6\text{-}Me_3C_6H_2)(CO)$ have been characterized by X-ray diffraction [47]. No evidence for isomerism was found in the formation of **11**.

As can be seen in the ORTEP views of **11** in Fig. 5, there is a large distortion present from the normally expected square planar geometries in the molecule. To the best of our knowledge, **11** represents only the second example of a structurally characterized Vaska's type compound with *cis*-geometry. The Ir atom, while approximately square-*coordinated*, is clearly not planar, and may be viewed as having a slight tetragonal distortion. This is almost certainly due in part to the intramolecular contacts between the *cis*-triphenylphosphine ligands. In Dahlenburg's *cis*-mesityl complex, a similar

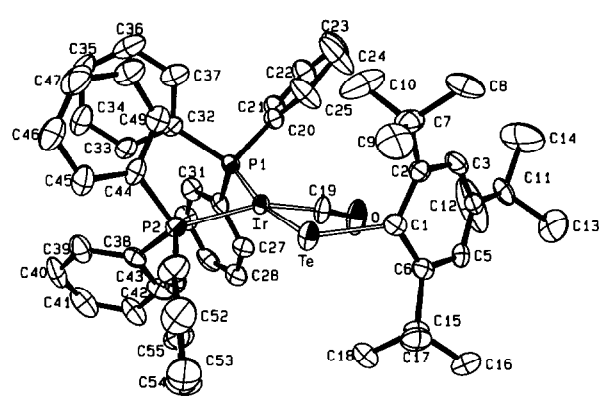

Fig. 5. ORTEP view of the molecular structure of *cis*-$(PPh_3)_2$-$Ir[Te(2,4,6\text{-}^tBu_3C_6H_2)](CO)$ (**11**). Thermal ellipsoids are scaled to represent the 50% probability surface.

TABLE 5. Selected bond distances (Å) and angles (deg) for **11**

Ir–Te	2.615(1)	Ir–P1	2.281(2)
Ir–P2	2.358(2)	Ir–C19	1.837(8)
C19–O	1.144(8)	Te–C1	2.170(7)
C1–C2	1.422(9)	C1–C6	1.42(1)
C2–C3	1.39(1)	C2–C7	1.55(1)
C3–C4	1.39(1)	C4–C5	1.40(1)
C4–C11	1.52(1)	C5–C6	1.394(9)
C6–C15	1.551(9)		
Te–Ir–P1	168.50(5)	Te–Ir–P2	88.12(5)
Te–Ir–C19	90.8(2)	P1–Ir–P2	97.28(6)
P1–Ir–C19	87.3(2)	P2–Ir–C19	161.0(2)
Ir–C19–O	172.9(7)	Ir–Te–C1	101.6(2)

tetragonal distortion is observed. Selected bond distances and angles for **11** are given in Table 5. The two Ir–P distances in **11** are significantly different (by 0.10 Å) as they are *trans* to two very different donors (Ir–P1, *trans* to Te, 2.281(2) Å; Ir–P2, *trans* to CO, 2.358(2) Å). Similarly, in *cis*-$(PPh_3)_2Ir(2,4,6\text{-}Me_3C_6H_2)(CO)$, the carbonyl moiety seems to be the stronger *trans* influence ligand as evidenced by the similar trend in Ir–P distances: Ir–P, *trans* to mesitylene, 2.324(3) Å; Ir–P, *trans* to CO, 2.370(3) Å. In the *trans*-isomer of Dahlenburg's mesityl Vaska's compound, the Ir–P distances are virtually identical at 2.313 and 2.319 Å [47]; this is also seen in a wide variety of other *trans* Vaska's type compounds: $(C_6F_6O)Ir(CO)(PPh_3)_2$, 2.320, 2.321 Å [48]; $PhOIr(CO)(PPh_3)_2$, 2.328, 2.344 Å [49]; $CH_3Ir(CO)(PPh_3)_2$, 2.300, 2.300 Å [50]; $[(3,5\text{-}(CF_3)_2\text{-pyrazolato-}N)]Ir(CO)(PPh_3)_2$, 2.328, 2.336 Å [51]. In **11**, both *trans* angles deviate from 180°; Te–Ir–P1 is 168.50(5)° while C19–Ir–P2 is 161.0(2)°. Additionally, the least squares plane containing Ir, Te, P1, and C19 show the four atoms to be co-planar to ±0.16 Å, while P2 is 1.11 Å out of this same plane. In addition, the tellurolate ligand is drastically distorted. The plane of the ligand is approximately perpendicular to the mean plane of the Ir atom. The *ipso* carbon is 0.26 Å out of the plane of the other five aromatic carbons, and the Te atom is 1.34 Å out of the same plane, in the direction of the Ir atom. The Ir–Te–C1 angle of 101.6(1)° is acute when compared to the Ir–O–C(*ipso*) angles of 126.5 and 135.4° for Atwood's *trans*-$PhOIr(CO)(PPh_3)_2$ [49] and *trans*-$(C_6F_6O)Ir(CO)(PPh_3)_2$ [48], respectively. The quaternary carbons of the *ortho* t-butyl groups are 0.33 and 0.30 Å out of the plane away from the Te, and the quaternary carbon of the *para* t-butyl group is 0.22 Å out of the plane toward the Te atom. The net effect is that the ligand has been bent into saddle shape. Some of this distortion may be due to packing forces between the molecules, as views of the unit cell and packing diagrams show good packing between the phosphine ligands, and seem to indicate that such molecular packing would not be nearly as favorable if the aryl tellurolate were not folded to some degree. Aryl–aryl contacts are visible across the inversion centers in the *a–b* plane, as are some contacts between the t-butyl groups and the phenyl rings of one of the PPh_3 ligands.

Reaction of **4** with 1/2 equiv. of $CdBr_2$ in THF affords the Cd tellurolate, **12**, as a yellow powder. Thermal decomposition leads to formation of a black powder (presumably CdTe) and the telluride, $(o\text{-}C_6H_4CH_2NMe_2)_2Te$. This mode of decomposition to a bis-organyltelluride and metal telluride was first observed by Steigerwald [11], and several other groups have reported similar reactions [18,19].

3. Experimental

3.1. General

Our standard operating procedures were as previously described [10]. Tellurium powder, $CdBr_2$ (Strem), n-butyl lithium (Aldrich or Johnson Matthey), N,N,N′,N′-tetramethylethylenediamine (TMEDA, Aldrich), *cis*-$(PPh_3)_2PtCl_2$ (Aldrich), and 1,3,5-tri-*iso*-propylbenzene (Lancaster Synthesis) were used as received. $LiEt_3BH$ and K^sBu_3BH (Aldrich) were used without further purification. 18-crown-6 (Strem) was recrystallized from acetonitrile and dried *in vacuo* overnight. Supermesitylene (1,3,5-tri-butylbenzene) (Aldrich) was brominated, and subsequently lithiated in a manner similar to that in the literature [52]. Literature methods were used to prepare $(2,4,6\text{-}Me_3C_6H_2)_2Te_2$ [53], $(2,4,6\text{-}^iPr_3C_6H_2)_2Te_2$ [15], and $Li(o\text{-}C_6H_4CH_2NMe_2)$ [54]. Melting points were determined in sealed capillaries under nitrogen. IR samples were prepared as Nujol mulls between KBr plates. ^1H, $^{13}C\{^1H\}$, and $^{31}P\{^1H\}$ NMR spectra were recorded at ambient temperatures. Chemical shifts (δ) for ^1H and $^{13}C\{^1H\}$ NMR spectra are relative to residual protium in the deuterated solvents listed, or relative to external 85% H_3PO_4 at δ 0.00 ppm in the $^{31}P\{^1H\}$ NMR data recorded. Routine C–H coupling constants are not reported. Elemental analyses were performed by the microanalytical laboratory of the College of Chemistry, University of California, Berkeley. MS analyses (EI or FAB) were performed by the Mass Spectrometry laboratory of the College of Chemistry, University of California, Berkeley. FAB MS was carried out using cesium as the atom source, nitrobenzyl alcohol (NBA) as the matrix, and with positive ion detection.

3.1.1. $(2,4,6\text{-}Me_3C_6H_2)TeLi(THF)_{1.5}$ (*1*)

A solution of $LiEt_3BH$ in THF (8.2 ml of a 1.0 M solution, 8.2 mmol) was added dropwise to a solution

of $(2,4,6\text{-}Me_3C_6H_2)_2Te_2$ (2.00 g, 4.1 mmol) in THF (70 ml). The dark red color quickly faded to pale yellow as the last few drops of the reductant were added, indicating complete conversion of the ditelluride to the tellurolate. The solution was stirred for 15 min, and the THF was removed under reduced pressure to afford 3.0 g (80%) of the product as a light beige powder that was pure enough to be used in subsequent reactions. Recrystallization from THF/pentane at −40°C overnight afforded clear, colorless prisms that lose THF on drying *in vacuo*. ^{1}H NMR (300 MHz, C_6D_6): δ 6.95 (s, 2H), 3.62 (m, 6 H), 2.88 (s, 6H), 2.19 (s, 3H), 1.31 (m, 6H).

3.1.2. $(2,4,6\text{-}^iPr_3C_6H_2)TeLi(THF)_{2.5}$ (2)

A THF solution of $LiEt_3BH$ (3.2 ml of a 1.0 M solution, 3.2 mmol) was added dropwise to a solution of $(2,4,6\text{-}^iPr_3C_6H_2)_2Te_2$ (1.07 g, 1.61 mmol). The solution was stirred for 15 min and the solvent was removed under reduced pressure. The resulting solid was crystallized from THF/pentane at −40°C to give 0.85 g (48%) of yellow-orange product. ^{1}H NMR (300 MHz, C_6D_6): δ 7.10 (s, 2H), 4.55 (heptet, 2H), 3.63 (m, 10H), 1.32 (d, 7H), 2.88 (heptet, 1H), 1.45 (d, 14H), 1.36 (m, 10H).

3.1.3. $(2,4,6\text{-}^tBu_3C_6H_2)TeLi(THF)_3$ (3)

The following is a modification of the method described by Du Mont [2]. THF (70 ml) was added to a mixture of Te powder (4 g, 30 mmol) and $(2,4,6\text{-}^tBu_3C_6H_2)Li(THF)_3$ (10.0 g, 21.4 mmol). The pale yellow mixture warmed slightly and became dark red as the tellurium dissolved. After 14 h, the solvent was removed under reduced pressure to give a red oil; this was triturated with pentane (100 ml) then extracted with two 100 ml portions of THF. The combined extracts were filtered, concentrated under vacuum and cooled to −40°C overnight to yield 7.0 g (56%) of yellow crystals that were isolated by filtration. The crystals appear to lose solvent at 112°C, then decompose at 250°C. NMR spectra were not obtained as the complex is insoluble in benzene-d_6 and reacts with $CDCl_3$. IR: 1590w, 1536w, 1407m, 1359s, 1237w, 1212w, 1178w, 1045s, 1000m, 916m, 889s, 874m, 741w, 672w, 355m, cm^{-1}. Anal. Calcd for $C_{30}H_{53}O_3LiTe$: C, 60.4; H, 8.96. Found: C, 60.6; H, 9.01%.

3.1.4. $(o\text{-}C_6H_4CH_2NMe_2)TeLi(DME)$ (4)

THF (100 ml) was added to a cold (−78°C) mixture of base free $(o\text{-}C_6H_4CH_2NMe_2)Li$ (4.0 g, 28 mmol) and tellurium (3.6 g, 28 mmol). The solution was allowed to warm to room temperature and was left to stir overnight. The dark orange solution was evaporated under vacuum to give a yellow oil that was triturated with hexane (20 ml) to give a yellow powder that was redissolved in DME (100 ml). The solution was filtered, concentrated to *ca.* 10 ml, and stored at −40°C for 12 h. Pale yellow needles (9.2 g, 91%) were isolated by filtration and dried under vacuum. M.p. 175–180°C (d). IR: 1574m, 1550w, 1378s, 1245s, 1198w, 1118m, 1084s, 1017m, 999s, 869s, 845w, 752s, 489m. ^{1}H NMR (300 MHz, C_6D_6): δ 8.83 (d, 1H), 6.99 (t, 1H), 6.91 (d, 1H), 6.75 (t, 1H), 3.65 (s, br, 2H), 2.74 (s, 4H), 2.73 (s, 6H), 1.94 (s, 6H). Anal. Calcd for $C_{13}H_{22}LiNO_2Te$: C, 43.5; H, 6.18; N, 3.90. Found: C, 43.6; H, 6.12; N, 3.81%.

3.1.5. $(2,4,6\text{-}Me_3C_6H_2)TeNa(TMEDA)_2$ (5)

A solution of $(2,4,6\text{-}Me_3C_6H_2)_2Te_2$ (1.25 g, 2.53 mmol) dissolved in THF (20 ml) was added to a Na/Hg amalgam (0.12 g, 5.2 mmol of Na in 10 g Hg). The deep red mixture was stirred for 20 min, over which time the color faded to give a pale yellow, clear solution. This was evaporated under reduced pressure, TMEDA (2 ml) and THF (10 ml) were added, and the solution was filtered and concentrated to *ca.* 4 ml. Cooling to −35°C for 24 h afforded yellow needles in 80% yield (2.0 g). M.p. 140°C (d). ^{1}H NMR (300 MHz, benzene-d_6/acetone-d_6, 10:1): δ 6.85 (s, 2H), 2.83 (s, 8H), 2.24 (s, 6H), 2.15 (s, 3H), 2.07 (s, 24H). Anal. Calcd. for $C_{21}H_{43}NaN_4Te$: C, 50.2; H, 8.63; N, 11.1. Found: C, 50.9; H, 8.51; N, 9.38%.

3.1.6. $(2,4,6\text{-}^iPr_3C_6H_2)TeNa(DME)$ (6)

A solution of $(2,4,6\text{-}^iPr_3C_6H_2)_2Te_2$ (1.50 g, 2.30 mmol) dissolved in THF (50 ml) was added to a Na/Hg amalgam (0.10 g, 4.5 mmol of Na in 10 g Hg). The mixture was stirred for 40 min, after which time the familiar dark red solution became yellow-orange. This solution was filtered away from the mercury, and the THF was removed under reduced pressure leaving the product as a yellow-orange solid. After washing with pentane and diethyl ether, the solid was extracted with DME (60 ml) and filtered. Pentane (20 ml) was added and the solution was cooled to −40°C for 24 h to afford the product as a yellow oil. This was dried at 10^{-2} Torr to give a yellow-orange powder, 1.26 g (64%). ^{1}H NMR (400 MHz, C_6D_6): δ 7.19 (s, 2H), 4.43 (s, br, 2H), 3.12 (s, 6H), 3.01 (s, 4H), 2.85 (heptet, 1H), 1.46 (d, 12H), 1.34 (d, 6H).

3.1.7. $(2,4,6\text{-}^iPr_3C_6H_2)TeK(THF)_{1.33}$ (7)

A solution of K^sBu_3BH in THF (6.0 ml of a 1.0 M solution, 6 mmol) was added dropwise to a solution of $(2,4,6\text{-}^iPr_3C_6H_2)_2Te_2$ (2.00 g, 3.02 mmol) in THF (40 ml). The solution was stirred for 15 min before the THF was removed under reduced pressure. The residue was extracted with THF (20 ml), filtered and concen-

trated to 5 ml before pentane (10 ml) was added. A light orange-yellow product quickly precipitated from solution. The mixture was cooled to −40°C for 12 h to produce 1.11 g (40%) of orange-yellow product. Crystallization via diffusion of pentane into a THF solution provided analytically pure samples of the polymeric potassium tellurolate. The clear, light yellow crystals begin to lose solvent at 93°C and slowly decompose between 215–230°C. IR: 1417s, 1236s, 1102s, 1054s, 1009s, 919m, 878m, 743m, 671s, 643s, 593s, 513s cm^{-1}. ^1H NMR (300 MHz, C_6D_6): δ 7.15 (s, 2H), 4.26 (heptet), 3.54 (m, 3H), 2.91 (heptet, 1H), 1.45 (d, 14H), 1.39 (m, 3H), 1.34 (d, 7H). Anal. Calcd for $C_{20.3}H_{33.6}KO_{1.3}Te$: C, 52.5; H, 7.29. Found: C, 52.1; H, 7.30%.

3.1.8. (2,4,6-$^iPr_3C_6H_2$)TeK(18-crown-6) (8)

Using a cannula, a THF solution of 18-crown-6 (0.135 g, 0.511 mmol in 10 ml) was added to a THF solution of **7** (0.300 g, 0.645 mmol in 10 ml). The mixture was stirred for 15 min and the solvent was removed under reduced pressure. The red-yellow solid was extracted with THF (5 ml). Slow vapor diffusion of pentane into the solution gave small, pale yellow needles, 0.15 g (47%), of the monomeric potassium tellurolate. The crystals become noticeably opaque at 135°C, and melt sharply from 219–221°C. IR: 1411s, 1349s, 1310s, 1299s, 1281s, 1251s, 1241s, 1114s, 1054s, 1006s, 964s, 837s, 325s cm^{-1}. ^1H NMR (500 MHz, C_6D_6): δ 7.13 (s, 2H), 5.05 (heptet, 2H), 3.11 (s, 24H), 2.96 (heptet, 1H), 1.56 (d, 12H), 1.40 (d, 6H). Anal. Calcd for $C_{27}H_{47}KO_6Te$: C, 51.1; H, 7.47. Found: C, 50.9; H, 7.58%.

3.1.9. cis-(PPh$_3$)$_2$Pt[Te(2,4,6-$^iPr_3C_6H_2$)]Cl (9)

Using a cannula, a THF solution of **2** (0.21 g, 0.38 mmol in 20 ml) was added to 0.30 g (0.38 mmol) of *cis*-$(PPh_3)_2PtCl_2$ suspended in THF (40 ml). Immediately, a pink-red solution formed. The reaction was allowed to stir overnight, and the THF was removed under reduced pressure. The solid was washed with pentane, and extracted with THF (20 ml). An equal volume of pentane was added and the solution was cooled to −40°C overnight. Filtration gave 0.29 g (70%) of the product as a hemi-THF solvate. The pink-red solid becomes a blood-red liquid from 170–175°C and then slowly begins to decompose. By 230°C, the material is a black liquid, and at 270°C a metallic mirror forms. IR: 3078w, 3044w, 1089w, 1068w, 1001w, 875w, 742m, 694m, 548m, 522m, 509m, 496w, cm^{-1}. ^1H NMR (300 MHz, C_6D_6): δ 7.75 (m, 7H), 7.49 (m, 7H), 7.21 (s, 2H), 6.86 (m, 16H), 4.75 (heptet, 2H), 3.57 (m, 4H), 2.86 (heptet, 1H), 1.60 (d, 12H), 1.41 (m, 4H), 1.25 (d, 6H). $^{31}P\{^1H\}$ (300 MHz, C_6D_6): AB pattern, δ 17.1, 16.8; $|^2J(PP)| = 17$ Hz, $|^1J(PPt)| = 2507$ Hz, $|^1J(PPt)| = 3876$ Hz. MS (F.A.B.): *m/z* 1085 (M^+), 1051 ($M^+ - Cl$), 993 [$Te_3(2,4,6\text{-}^iPr_3C_6H_2)_3^+$], 7.55 [$(PPh_3)_2PtCl$], 718 [$(PPh_3)_2Pt$], 662 [$Te_2(2,4,6\text{-}^iPr_3C_6H_2)_2$], 330 [$Te(2,4,6\text{-}^iPr_3C_6H_2)$]. UV-vis ($CH_3CN$, 3.6×10^{-4} M): λ_{max} 500 nm ($\epsilon = 563$ l mol^{-1} cm^{-1}). Anal. Calcd for $C_{53}H_{57}ClO_{0.5}P_2PtTe$: C, 56.7; H, 5.1. Found: C, 56.7; H, 5.0%.

3.1.10. cis-(PPh$_3$)$_2$Pt[Te(2,4,6-$^tBu_3C_6H_2$)]Cl (10)

Using a cannula, a THF solution of **3** (0.45 g, 0.76 mmol in 20 ml) was added to 0.60 g (0.76 mmol) of *cis*-$(PPh_3)_2PtCl_2$ suspended in THF (40 ml). The resulting deep purple solution was allowed to stir for 30 min, and the THF was removed under reduced pressure. The purple product was extracted with 100 ml of toluene, filtered, and concentrated (30 ml). Pentane (30 ml) was added and the solution was cooled to −40°C for 18 h. Filtration afforded small, air stable, red-purple crystals, 0.75 g (88%). Alternatively, crystallization from a dichloromethane/diethyl ether solvent system via slow vapor diffusion at 0°C for 10 days provided analytically pure material as a hemi-dichloromethane solvate. The crystals obtained from toluene/pentane begin to lose solvent at 113°C. Noticeable decomposition begins at 160°C, and at 247°C, the material is a black liquid. IR: 3071s, 3053s, 1433s, 1092s, 1001s, 873s, 733s, 696m, 544s, 514s, 495s, 419s cm^{-1}. ^1H NMR (300 MHz, $CDCl_3$): δ 7.61 (m, 7H), 7.16 (m, 20H), 6.99 (m, 5H), 1.76 (s, 18H), 1.18 (s, 9H). $^{31}P\{^1H\}$ NMR (300 MHz, $CDCl_3$): AB pattern, δ 17.4, 16.7; $|^2J(PP) = 18$ Hz, $|^1J(PPt)| = 2478$ Hz, $|^1J(PPt)| = 3934$ Hz. UV-vis (CH_3CN, 4.2×10^{-4}M): λ_{max} 536 nm ($\epsilon = 676$ l mol^{-1} cm^{-1}). Anal. Calcd for $C_{54.5}H_{60}ClP_2PtTe$: C, 55.7; H, 5.14. Found: C, 56.1; H, 5.13%.

3.1.11. cis-(PPh$_3$)$_2$Ir[Te(2,4,6-$^tBu_3C_6H_2$)](CO) (11)

Diethyl ether (20 ml) was added to a mixture of *trans*-$(PPh_3)_2Ir(CO)Cl$ (0.30 g, 0.38 mmol) and **3** (0.22 g, 0.38 mmol). The mixture was stirred for 8 h, the volatiles were evaporated, and the red residue was extracted into toluene (10 ml) and filtered. The solution was concentrated to *ca.* 3 ml, 3 ml of pentane was added, and the mixture was cooled to −40°C. Large red needles (*m.p.* 175–176°C) were isolated by filtration after 24 h. Yield 0.27 g, 80%. IR: ν(CO) 1967. ^1H NMR (C_6D_6, 300 MHz): δ 7.57 (m, 12H), 6.87 (m, 18H), 2.11 (s, 18H), 1.33 (s, 9H). $^{31}P\{^1H\}$ NMR (C_6D_6, 300 MHz): δ 28.6 (s, br), 19.8 (s, br). Anal. Calcd for $C_{55}H_{59}IrOP_2Te$: C, 59.1; H, 5.32. Found: C, 58.8; H, 5.38%.

3.1.12. Cd[Te(o-C$_6$H$_4$CH$_2$NMe$_2$)]$_2$ (12)

THF (20 ml) was added to a mixture of **4** (0.79 g, 2.2 mmol) and $CdBr_2$ (0.30 g, 1.1 mmol) at room tempera-

ture. The orange-yellow homogeneous solution was stirred for 4 h before removing the volatiles by vacuum distillation. The yellow oil was triturated with hexane (20 ml) to give a yellow powder that was dissolved in toluene (10 ml). The solution was concentrated to *ca.* 2 ml and hexane (2 ml) was added dropwise with shaking. The solution was cooled to −40°C overnight to afford the product as a yellow powder in 85% yield (0.20 g, m.p. 148–149°C). ^{1}H NMR ($CDCl_3$, 400 MHz): δ 8.47 (d, 1H), 7.05 (t, 1H), 6.92 (m, 2H), 3.56 (s, br, 2H), 2.29 (s, br, 6H). $^{13}C\{^1H\}$ NMR: 143.5, 141.0, 131.1, 128.5, 126.1, 111.0, 71.4, (methyl carbon not detected). Anal. Calcd for $C_{18}H_{24}CdN_2Te_2$: C, 34.0; H, 3.80; N, 4.40. Found: C, 34.4; H, 2.90; N, 4.40%. The highest mass observed by EI MS corresponded to the telluride, $(o\text{-}C_6H_4CH_2NMe_2)_2Te$, below.

3.1.12.1. Thermal decomposition of **12**. A small amount of **12** was placed in a vacuum sublimator and heated to 180°C at 1 mm Hg pressure. A white solid, $(o\text{-}C_6H_4CH_2NMe_2)_2Te$, sublimed onto the water-cooled probe and a black powder remained behind. For $(o\text{-}C_6H_4CH_2NMe_2)_2Te$: MS (EI): 398 ($M^+$). ^{1}H NMR ($CDCl_3$, 400 MHz): δ 7.55 (d, 1H), 7.19 (d, 1H), 7.12 (t, 1H), 6.95 (t, 1H), 3.53 (s, 2H), 2.29 (s, 6H). $^{13}C\{^1H\}$ NMR: 142.5, 138.5, 128.6, 127.5, 126.4, 118.0, 67.1, 44.2.

3.2. X-Ray structural studies

For **3**, **10**, and **11**, crystal quality was examined through Laue photographs prior to mounting the compounds on an Enraf-Nonius CAD-4 diffractometer. The accurate cell dimensions for each compound were derived by a least-squares fit to the setting angles of the unresolved Kα components of 12 reflections (for **3**), 24 reflections (for **4**, **10**, and **11**), or 25 reflections (for **7**) obtained via automatic peak search and indexing procedures. Niggli values in each case were inspected and revealed no conventional cells of higher symmetry, other than those chosen. Intensity standards for each compound were measured on the diffractometer using graphite-monochromated Mo Kα radiation every one hour of data collection. For each compound, no significant decrease in intensity was observed during the data collection periods. All raw intensity data were converted to structure factor amplitudes by correction for scan speed, background and Lorentz and polarization effects. Appropriate absorption corrections were made for each compound. Each structure, except that of **7**, was solved by Patterson methods and refined via standard least-squares and Fourier techniques. The structure of **7** was solved by direct methods using the SHELXS-8 program [55]. The quantity minimized by the least-squares program was $\Sigma w(|F_o| - |F_c|)^2$, where w is the weight of a given

TABLE 6. Crystallographic data for compounds

	3	**4**	**7**	**10**	**11**
Formula	$C_{30}H_{53}LiO_3Te$	$C_{13}H_{22}LiNO_2Te$	$C_{61}H_{98}K_3O_4Te_3$	$C_{54}H_{59}ClP_2PtTe$	$C_{55}H_{59}IrOP_2Te$
Mol weight	596.3	358.9	1395.6	1128.2	1117.8
Space group	$P2_1/c$	$P2_1/n$	$P\bar{1}$	$P2_1/c$	$P\bar{1}$
a, Å	18.317(3)	8.442(1)	13.225(2)	10.555(4)	9.879(3)
b, Å	10.753(2)	13.153(2)	15.492(3)	18.182(5)	15.031(4)
c, Å	17.983(3)	14.428(2)	19.099(2)	27.915(5)	18.137(4)
α, deg	90.0	90.0	76.56(1)	90.0	69.63(2)
β, deg	114.90(1)	92.11(1)	72.17(1)	94.36(2)	80.27(2)
γ, deg	90.0	90.0	67.18(2)	90.0	72.90(2)
Vol, Å^3	3213(2)	1601.0(7)	3404.8(8)	5342(5)	2406(1)
Z	4	4	2	4	2
ρ_{calcd}, g cm^{-3}	1.23	1.49	1.36	1.40	1.54
Crystal size, mm	0.20 × 0.20 × 0.30	0.20 × 0.30 × 0.35	0.15 × 0.25 × 0.40	0.10 × 0.16 × 0.30	0.08 × 0.08 × 0.35
Radiation, Å	Mo K_α 0.71073	Mo K_α 0.70926	Mo K_α 0.70926	Mo K_α 0.70926	Mo K_α 0.71073
Scan mode	θ–2θ	θ–2θ	ω	ω	θ-2θ
2θ range, deg	3–45	3–45	3–45	3–45	3–45
Collection range	$+h, +k, \pm l$	$+h, +k, \pm l$	$+h, \pm k, \pm l$	$+h, +k, \pm l$	$+h, \pm k, \pm l$
Absorption coeff	$\mu = 9.5$	$\mu = 18.5$	$\mu = 15.0$	$\mu = 33.3$	$\mu = 34.6$
No. of unique reflns	4187	2083	8882	6901	6291
Reflns $w/F^2 > 3\sigma(F^2)$	2716	1821	5564	4646	5060
Final R, R_w	0.0371, 0.0395	0.0200, 0.0237	0.0366, 0.0379	0.044, 0.044	0.0320, 0.0365
T, °C	−82	−87		−95	−80

observation. Hydrogen atoms were assigned idealized locations and were included in structure factor calculations, but were not refined. There was no indication of secondary extinction in the high-intensity low angle data for either of the compounds. A summary of data collection and refinement parameters is given in Table 6. The structure of each compound was determined by Dr. F.J. Hollander at the U.C. Berkeley College of Chemistry X-ray facility, CHEXRAY.

3.2.1. Compound 3

Pale, brown-yellow crystals were obtained by slow crystallization from THF at −40°C. Fragments cleaved from some of these crystals were mounted on glass fibers using polycyanoacrylate cement. The crystal used for data collection was centered and cooled to −82°C. The unit cell was determined to be primitive monoclinic with space group $P2_1/c$. Removal of the systematically absent and redundant data left 4187 unique data in the final data set. Just prior to the final refinement, 25 reflections which were apparently affected by crystal misorientation, were removed from the data set. The largest peak in the final difference Fourier map had an electron density of 0.31 e Å^{-3}, and the lowest excursion was −0.46 e Å^{-3}. The final residuals for 316 variables refined against the 2716 accepted data for which $F^2 > 3\sigma(F^2)$ were R = 0.0371, $R_w = 0.0395$, and GOF = 1.44. The R value for all 4162 data was 0.095.

3.2.2. Compound 4

Large, clear, pale-yellow crystals were obtained by slow crystallization from DME at −40°C. A fragment cleaved from one of these crystals was mounted on a glass fiber using Paratone N hydrocarbon oil. The crystal was centered and cooled to −87°C. The unit cell was determined to be primitive monoclinic with space group $P2_1/n$. Removal of the systematically absent and redundant data left 2083 unique data in the final data set. The largest peak in the final difference Fourier map had an electron density of 0.45 e$^-$ Å^{-3}, and the lowest excursion was −0.38 e$^-$ Å^{-3}. The final residuals for 163 variables refined against the 1821 data for which $F^2 > 3\sigma(F^2)$ were $R = 0.0200$, $R_w = 0.0237$, and GOF = 1.54. The R value for all 2083 data was 0.0265.

3.2.3. Compound 7

Large, clear, columnar crystals were obtained by slow vapor diffusion of pentane into a THF solution of the compound. A fragment cleaved from one of these crystals was mounted on a glass fiber using Paratone N hydrocarbon oil and was then centered and cooled to −120°C. The unit cell was determined to be primitive triclinic with space group $P\bar{1}$. The largest peak in the final difference Fourier map had an electron density of 0.56 e Å^{-3}, and the lowest excursion was −0.10 e Å^{-3}. The final residuals for 640 variables refined against the 5,564 accepted data for which $F^2 > 3\sigma(F^2)$ were $R = 0.0366$, $R_w = 0.0379$, and GOF = 1.307. The R value for all 8,882 data was 0.1005.

3.2.4. Compound 10

Purple, rodlike crystals were obtained by slow diffusion of pentane into a toluene solution of the compound at −40°C. A fragment cleaved from one of these crystals was mounted on a glass fiber using polycyanoacrylate cement, centered in the beam, and cooled to −95°C. The unit cell was determined to be primitive monoclinic with space group $P2_1/c$. Removal of the systematically absent and redundant data left 6901 unique data in the final data set. The largest peak in the final difference Fourier map had an electron density of 1.49 e$^-$ Å^{-3}, and the lowest excursion was −0.29 e$^-$ Å^{-3}. The largest peaks were located 1.8 Å from two of the methyl carbons of one of the t-butyl ligands. The final residuals for 595 variables refined against the 4676 data for which $F^2 > 3\sigma(F^2)$ were $R = 0.0464$, $R_w = 0.0509$, and GOF = 1.71. The R value for all 6901 data was 0.0870.

3.2.5. Compound 11

Clear, red, columnar crystals were obtained by slow crystallization from toluene/pentane at −40°C. Fragments cleaved from some of these crystals were mounted on glass fibers using polycyanoacrylate cement. A crystal was centered and cooled to −80°C. The unit cell was determined to be primitive triclinic with space group $P\bar{1}$. Just prior to the final refinement, 84 data which were apparently collected while the crystal was misoriented were given zero weights. The largest peak in the final difference Fourier map had an electron density of 1.12 e Å^{-3}, and the lowest excursion was −0.22 e Å^{-3}. The largest peaks were located near the Ir and Te atoms. The final residuals for 541 variables refined against the 5060 accepted data for which $F^2 > 3\sigma(F^2)$ were $R = 0.0320$, $R_w = 0.0365$, and GOF = 1.39. The R value for all 6207 data was 0.0449.

Acknowledgements

We thank the Donors of the Petroleum Research Fund, administered by the American Chemical Society, for partial support of this work and the US Department of Education for a fellowship to P.J.B.

Note added in proof

Another example of a chelating lithium tellurolate salt was reported very recently. See: H. Gornitzka, S. Besser, R. Herbst-Irmer, U. Kilimann and F.T. Edelmann, *Angew. Chem., Int. Ed. Engl., 31* (1992) 1261

References

1 H. J. Gysling, *Coord. Chem. Rev., 42* (1982) 133.
2 L. Lange and W.-W. Du Mont, *J. Organomet. Chem., 286* (1985) C1.
3 H. J. Gysling, in S. Patai and Z. Rappoport (eds.), *The Chemistry of Organic Selenium and Tellurium Compounds*, Wiley, New York, 1986, p. 679.
4 C. Köllemann, D. Obendorf and F. Sladky, *Phosphorus and Sulfur, 38* (1988) 69.
5 B. Bildstein, K. Giselbrecht and F. Sladky, *Chem. Ber., 122* (1989) 2279.
6 P. J. Bonasia and J. Arnold, *J. Chem. Soc., Chem. Commun.*, (1990) 1299.
7 W.-W. Du Mont, S. Kubiniok, L. Lange, S. Pohl, W. Saak and I. Wagner, *Chem. Ber., 124* (1991) 1315.
8 K. Ruhlandt-Senge and P. P. Power, *Inorg. Chem., 30* (1991) 3683.
9 P. J. Bonasia and J. Arnold, *Inorg. Chem., 31* (1992) 2508.
10 P. J. Bonasia, D. E. Gindelberger, B. O. Dabbousi and J. Arnold, *J. Am. Chem. Soc., 114* (1992) 5209.
11 M. L. Steigerwald and C. R. Sprinkle, *J. Am. Chem. Soc., 109* (1987) 7200.
12 M. L. Steigerwald and C. R. Sprinkle, *Organometallics, 7* (1988) 245.
13 J. G. Brennan, T. Siegrist, P. J. Carroll, S. M. Stuczynski, L. E. Brus and M. L. Steigerwald, *J. Am. Chem. Soc., 111* (1989) 4141.
14 J. G. Brennan, T. Siegrist, P. J. Carroll, S. M. Stuczynski, P. Reynders, L. E. Brus and M. L. Steigerwald, *Chem. Mater., 2* (1990) 403.
15 M. Bochmann, A. P. Coleman, K. J. Webb, M. B. Hursthouse and M. Mazid, *Angew. Chem., Int. Ed. Engl., 30* (1991) 973.
16 M. Bochmann and K. J. Webb, *J. Chem. Soc., Dalton Trans.*, (1991) 2325.
17 M. Bochmann, K. J. Webb, M. B. Hursthouse and M. Mazid, *J. Chem. Soc., Dalton Trans.*, (1991) 2317.
18 M. Bochmann, K. Webb, M. Harman and M. B. Hursthouse, *Angew. Chem., Int. Ed. Engl., 29* (1990) 638.
19 A. R. Strzelecki, P. A. Timinski, B. A. Helsel and P. A. Bianconi, *J. Am. Chem. Soc., 114* (1992) 3159.
20 J. Arnold, J. M. Walker, K. M. Yu, P. J. Bonasia, A. L. Seligson and E. D. Bourret, *J. Cryst. Growth, 124* (1992) 647.
21 M. Bochmann, A. P. Coleman, K. J. Webb, M. B. Hursthouse and M. Mazid, *Angew. Chem., Int. Ed. Engl., 30* (1991) 973.
22 M. Bochmann, K. Webb, M. Harman and M. B. Hursthouse, *Angew. Chem., Int. Ed. Engl., 29* (1990) 638.
23 K. J. Irgolic, *The Organic Chemistry of Tellurium*, Gordon and Breach, New York, 1974.
24 J. Liesk, P. Schulz and G. Klar, *Z. Anorg. Allg. Chem., 435* (1977) 98.
25 W.-W. Du Mont, R. Hensel and S. Kubiniok, *Phosphorus and Sulfur, 38* (1988) 85.
26 C. H. W. Jones and R. D. Sharma, *J. Organomet. Chem., 255* (1983) 61.
27 H. J. Gysling and H. R. Luss, *Organometallics, 3* (1984) 596.
28 T. Kemmitt and W. Levason, *Organometallics, 8* (1989) 1303.
29 A. K. Singh and V. Srivastava, *J. Coord. Chem., 21* (1990) 39.
30 A. K. Singh, V. Srivastava and B. L. Khandelwal, *Polyhedron, 9* (1990) 495.
31 R. D. Shannon and C. T. Prewitt, *Acta Crystallogr., B25* (1969) 925.
32 T. G. Appleton and M. A. Bennett, *Inorg. Chem., 17* (1978) 738.
33 T. G. Appleton, H. C. Clark and L. E. Manzer, *Coord. Chem. Rev., 10* (1973) 335.
34 R. Bardi and A. M. Piazzesi, *Inorg. Chim. Acta, 47* (1981) 249.
35 J. A. Kaduk and J. A. Ibers, *J. Organomet. Chem., 139* (1977) 199.
36 W. Conzelmann, J. D. Koola, U. Kunzee and J. Strahle, *Inorg. Chim. Acta, 89* (1984) 147.
37 D. R. Russell and P. A Tucker, *J. Chem. Soc., Dalton Trans.*, (1975) 2222.
38 B. L. Khandelwal, K. Kundu and S. K. Gupta, *Inorg. Chim. Acta, 154* (1988) 183.
39 B. L. Khandelwal and S. K. Gupta, *Inorg. Chim. Acta, 166* (1989) 199.
40 D. M. Giolando, T. B. Rauchfuss and A. L. Rheingold, *Inorg. Chem., 26* (1987) 1636.
41 V. K. Jain, S. Kannan and R. Bohra, *Polyhedron, 11* (1992) 1551.
42 R. D. Adams, T. A. Wolfe, B. W. Eichhorn and R. C. Haushalter, *Polyhedron, 8* (1989) 701.
43 L. Dahlenburg and R. Nast, *Angew. Chem., Int. Ed. Engl., 15* (1976) 110.
44 L. Dahlenburg, V. Sinnwell and D. Thoennes, *Chem. Ber., 111* (1978) 3367.
45 L. Dahlenburg and F. Mirzaei, *J. Organomet. Chem., 173* (1979) 325.
46 L. Dahlenburg, F. Mirzaei and A. Yardimcioglu, *Z. Naturforsch., Teil B, 87* (1982) 310.
47 L. Dahlenburg, K. Von Deuten and J. Kopf, *J. Organomet. Chem., 216* (1981) 113.
48 M. R. Churchill, J. C. Fettinger, W. M. Rees and J. D. Atwood, *J. Organomet. Chem., 308* (1986) 361.
49 W. M. Rees, M. R. Churchill, J. C. Fettinger and J. D. Atwood, *Organometallics, 4* (1985) 2179.
50 W. M. Rees, M. R. Churchill, Y. J. Li and J. D. Atwood, *Organometallics, 4* (1985) 1162.
51 A. L. Bandini, G. Banditelli, F. Bonati, F. Demartin, M. Manassero and G. Minghetti, *J. Organomet. Chem., 238* (1982) C9.
52 D. E. Pearson, M. G. Frazer, V. S. Frazer and L. C. Washburn, *Synthesis*, (1976) 621.
53 W. S. Haller and K. J. Irgolic, *J. Organomet. Chem., 38* (1972) 97.
54 J. T. B. H. Jastrzebski and G. Van Koten, *Inorg. Synth., 26* (1989) 152.
55 G. M. Sheldrick, *Crystallographic Computing 3*, Oxford University Press, 1985.